Universality classes of the domain-wall creep motion driven by spin-transfer torques

M. H. Jin,[1] L. Xiong,[2,3] N. J. Zhou,[4] B. Zheng,[2,3,5,*] and T. J. Zhou[1,†]

[1]*College of Electronics and Information, Hangzhou Dianzi University, Hangzhou 310018, People's Republic of China*

[2]*School of Physics and Astronomy, Yunnan University, Kunming 650091, People's Republic of China*

[3]*Department of Physics, Zhejiang University, Hangzhou 310027, People's Republic of China*

[4]*Department of Physics, Hangzhou Normal University, Hangzhou 310036, People's Republic of China*

[5]*Collaborative Innovation Center of Advanced Microstructures, Nanjing University, Nanjing 210093, People's Republic of China*

(Received 26 December 2020; accepted 27 May 2021; published 14 June 2021)

With the stochastic Landau-Lifshitz-Gilbert equation, we numerically simulate the creep motion of a magnetic domain wall driven by the adiabatic and nonadiabatic spin-transfer torques induced by the electric current. The creep exponent μ and the roughness exponent ζ are accurately determined from the scaling behaviors. The creep motions driven by the adiabatic and nonadiabatic spin-transfer torques belong to different universality classes. The scaling relation between μ and ζ based on certain simplified assumptions is valid for the nonadiabatic spin-transfer torque, while invalid for the adiabatic one. Our results are compatible with the experimental ones, but go beyond the existing theoretical prediction. Our investigation reveals that the disorder-induced pinning effect on the domain-wall rotation alters the universality class of the creep motion.

DOI: 10.1103/PhysRevE.103.062119

I. INTRODUCTION

Magnetic domain walls have attracted considerable attention because of the academic interest in a nonlinear dynamic system and the potential applications in data storage, spin logic devices, neuromorphic computing, etc. [1–5]. The key in these applications is to effectively control the displacement and the velocity of the domain wall. In addition to the domain-wall motion driven by the magnetic field, various theoretical and experimental efforts in recent years have been devoted to manipulating the domain walls with the spin-transfer torque (STT) induced by the electric current [6–9]. The STT-driven domain-wall motion is quite distinct from the field-driven one. For example, the domain wall in certain parameter regimes is intrinsically pinned at zero temperature, even in the absence of disorder [8–10]. From the view of applications, the STTs drive the domain walls more efficiently, with a lower energy consumption [11–14]. The domain-wall motion is sensitive to impurities, notches, and defects in magnetic materials. The disorder may greatly reduce the domain-wall mobility and induce the domain-wall roughening. Therefore, it is particularly important to understand the mechanism of the current-driven domain-wall motion in the disordered medium.

At zero temperature, the domain-wall motion driven by an external driving force f exhibits a pinning-depinning phase transition induced by the disorder. The depinning threshold f_c separates a zero-velocity regime for $f < f_c$ and a finite-velocity regime for $f > f_c$. At the nonzero temperatures, however, the creep motion of the domain wall is activated, even when the driving force f is far below the depinning threshold f_c. In the creep regime $f \ll f_c$, the domain-wall velocity v obeys an Arrhenius scaling law $\log(v) \sim f^{-\mu}$, where μ is the so-called creep exponent. It is well known that the creep motion of the domain wall driven by the magnetic field is categorized into a universality class with the random bond or the random field, which is characterized by $\mu = 0.25$ or 1, respectively [15–21]. Since the interaction of the domain wall with the STT is essentially different from that with the magnetic field, the universality class for the creep motion of the STT-driven domain wall remains controversial. The theoretical analyses and the experimental measurements report different values of the creep exponents [22–25].

The pinning-depinning phase transition and the creep motion of the magnetic topological defects, such as domain walls, vortices, and skyrmions, have been intensively investigated [26–36]. It has been found that the STT, especially an adiabatic one, plays a novel role in the pinning-depinning phase transition and changes the universality classes [28,30]. Nonetheless, how the STT affects the creep motion and the creep exponent of the domain wall is still ambiguous [24,25]. In most experimental works on the creep motion of the current-driven domain wall, the adiabatic and nonadiabatic effects of the driving currents are not strictly distinguished [37–39]. Usually, the theoretical value $\mu = 0.25$ or 1 of the creep exponent is taken as an input to verify the Arrhenius scaling law in the experiments as well as the numerical simulations, and independent measurements of the creep exponent are scarce [40–44].

Compared to the simplified statistical models, the stochastic Landau-Lifshitz-Gilbert (sLLG) equation is more fundamental to the description of the spin dynamics of magnetic systems at finite temperatures. The adiabatic and nonadiabatic

*Corresponding author: zhengbo@zju.edu.cn

†Corresponding author: tjzhou@hdu.edu.cn

STTs derived from the spin-diffusion model can be explicitly introduced in this equation to investigate the current-driven domain-wall motion [6,8]. The numerical and theoretical results based on the sLLG equation are in good agreement with the experimental ones and even provide reasonable predictions [8,26–28]. Various properties of the magnetic systems have been studied recently with the sLLG equation, such as the thermal magnetization switching process, the magnonic spin Seebeck effect, and spin-wave excitation [45–54]. However, due to the time-consuming computation and the complexity of the sLLG equation, the universal dynamic behaviors at nonzero temperatures are rarely investigated.

In this paper we perform a large-scale numerical simulation of the sLLG equation to investigate the creep motion of the domain wall driven by the STTs in a disordered film. The creep exponent μ and the roughness exponent ζ for the adiabatic and nonadiabatic STTs are accurately measured from the scaling behaviors. Our numerical results are comprehensively analyzed and compared with the existing experimental and theoretical ones. In Sec. II the model and the scaling behaviors are described. In Sec. III the numerical simulations are carried out to evaluate the exponents for the creep motion of the STT-driven domain-wall motion. A summary is given in Sec. IV.

II. MODEL AND SCALING BEHAVIORS

A. Landau-Lifshitz-Gilbert equation

The sLLG equation with the STTs along the x axis describes the microscopic dynamics of the magnetic system at a finite temperature [6,8,55],

$$\frac{\partial \mathbf{m}_i}{\partial t} = -\mathbf{m}_i \times \mathbf{h}_{\mathrm{eff},i} + \alpha \mathbf{m}_i \times \frac{\partial \mathbf{m}_i}{\partial t} - u\frac{\partial \mathbf{m}_i}{\partial x} + bu\mathbf{m}_i \times \frac{\partial \mathbf{m}_i}{\partial x}, \tag{1}$$

where $\mathbf{m}_i = \mathbf{M}_i/M_s$ is the unit vector of the local magnetization on site i, M_s is the saturation magnetization, and α is the Gilbert damping constant. The last two terms on the right-hand side of the equation are the adiabatic and nonadiabatic STTs, respectively, and the strength of the nonadiabatic STT is determined by the coefficient b. In addition, $u = JPg\mu_B/2eM_s$ is the magnitude of the driving current along the x axis, where J, P, e, g, and μ_B are the current density, the polarization rate, the electron charge, the g factor, and the Bohr magneton, respectively.

The effective field is

$$\mathbf{h}_{\mathrm{eff},i} = A\nabla^2\mathbf{m}_i + K_\parallel m_{x,i}\mathbf{e}_x - K_\perp m_{z,i}\mathbf{e}_z + \mathbf{h}_{\mathrm{th},i} + \mathbf{h}_{d,i}, \tag{2}$$

where the stochastic thermal fields induced by the temperature T are introduced via the white Gaussian noises [56],

$$\langle \mathbf{h}_{\mathrm{th},i}(t) \cdot \mathbf{h}_{\mathrm{th},j}(t')\rangle = \frac{2\alpha k_B T}{\mu_0 \mu_s \gamma_0}\delta_{ij}\delta(t-t'). \tag{3}$$

Here γ_0 is the gyromagnetic ratio, μ_s is the magnetic moment, T is the temperature, and $A = J_{\mathrm{ex}}/\mu_0 M_s^2 d^2$ is the exchange coefficient with the lattice constant d. In addition, $K_\parallel = D_\parallel/\mu_0 M_s^2$ and $K_\perp = D_\perp/\mu_0 M_s^2$ are the easy-axis and hard-axis anisotropy coefficients, respectively. The thermal field $\mathbf{h}_{\mathrm{th},i}$ and the quenched disorder $\mathbf{h}_{d,i}$ in Eq. (2) are normalized by the saturation magnetization, i.e., $\mathbf{h}_{d,i} = \mathbf{H}_{d,i}/M_s$ and $\mathbf{h}_{\mathrm{th},i} = \mathbf{H}_{\mathrm{th},i}/M_s$. In other words, the parameters are set to be dimensionless. The time, length, and energy density are measured in units of $(\gamma_0 M_s)^{-1}$, $\pi\sqrt{A/K_\parallel}$, and $\mu_0 M_s^2$, respectively [26,36,52]. Theoretically, we suppose that the creep motion of the domain wall is investigated in the thermodynamic limit. Thus, the simulation system should be regarded as an infinite magnetic film and sufficiently large lattice sizes should be used to ensure that the finite-size effect is ignorable. It is shown that the magnetostatic interaction is mathematically equivalent to an easy-plane anisotropy or a hard-axis perpendicular anisotropy for an infinite film [6,57]. For simplicity, the magnetostatic interaction is replaced by the hard-axis perpendicular anisotropy in our model.

B. Scaling behaviors of creep motion

Since the x component of the magnetization vector $\mathbf{m}_i$ changes its value from 1 to -1 across the domain wall, the domain-wall position $h(y)$ is determined by the minimum absolute value of m_x at each y. The average velocity of the domain wall is thus calculated by

$$v(t) = \frac{d\langle h(y,t)\rangle}{dt}, \tag{4}$$

where $\langle\cdots\rangle$ represents both the statistical average and the average in the y direction.

The roughness function of the domain wall is defined by

$$C(L) = \langle [h(y+L) - h(y)]^2\rangle, \tag{5}$$

where L is the length of the domain-wall segment along the y axis, and it describes the spatial correlation of the domain-wall position in the y direction. Based on the functional renormalization group theory in the equilibrium state without the driving force, the roughness function $C(L)$ obeys the scaling behavior [58]

$$C(L) \sim L^{2\zeta}, \tag{6}$$

where ζ is the equilibrium roughness exponent.

In the creep regime of the domain-wall motion, the current-velocity Arrhenius scaling law is expected to be [15–21]

$$v = v_0 \exp\left[-\frac{E_c}{k_B T}\left(\frac{u_c}{u}\right)^\mu\right], \tag{7}$$

where u_c is the depinning current at zero temperature, v_0 is the velocity at u_c, E_c is the characteristic energy scale, and $k_B T$ is the thermal energy scale.

A scaling relation between the creep exponent and the equilibrium roughness exponent has been derived from the theoretical analysis based on the sLLG equation under certain assumptions or approximations [22,23], and for $b = 0$,

$$\mu_a = \frac{2\zeta - 1}{2 - 2\zeta}, \tag{8}$$

while for $b \neq 0$,

$$\mu_n = \frac{2\zeta - 1}{2 - \zeta}. \tag{9}$$

Here μ_a and μ_n denote the creep exponents of the adiabatic and nonadiabatic STTs, respectively.

III. NUMERICAL SIMULATION

The model parameters without the normalization, i.e., the exchange constant, anisotropy constant, lattice constant, and saturation magnetization, are chosen to be $J_{\rm ex} = 2.99 \times 10^{-12}$J/m, $D_{\parallel} = 1.06 \times 10^{5}$J/m^3, $D_{\perp} = 1.06 \times 10^{4}$J/m^3, $d = 1.68 \times 10^{-9}$ m, and $M_s = 9.2 \times 10^{5}$A/m, mainly following the parameters of the FePt materials [26–28]. The experimental value of the damping constant varies in a wide regime, from $\alpha = 0.001$ to 4.0 in different materials [43,52,53]. A smaller α leads to a larger velocity of the domain wall and a stronger fluctuation, and larger lattice sizes and more samples for the statistical average are required. In order to obtain reliable results in a reasonable simulation time, we set $\alpha = 1$ in our simulations. Additional simulations for $\alpha = 0.5$ are also performed to verify the important results, such as the creep exponent and roughness exponent. The direction of the quenched disorder $\mathbf{h}_{d,i}$ is randomly and uniformly distributed in the unit spherical space, while the amplitude is uniformly distributed within an interval $[-\Delta, \Delta]$ with $\Delta = 0.5$. In our simulations, the strength of the quenched disorder is not large; thus the spins in the bulk, i.e., the spatial region outside the domain wall, almost do not evolve with time at zero temperatures and with only some random fluctuations at nonzero temperatures. We set the temperature to be $T = 200$, 250, and 300 K, respectively. At these temperatures, the thermal effect is much larger than the pinning effect induced by the quenched disorder. Therefore, the dynamic system can successively overcome the potential barriers, resulting in the creep motion of the domain wall. The typical value of the nonadiabatic coefficient b is 0.01–0.1 in experiments. In our simulation, we set $b = 0.1$. If only the adiabatic STT is applied, i.e., $b = 0$, there exists an intrinsic pinning potential in the absence of disorder and therefore the domain wall is pinned below a certain threshold [8–10]. When both the adiabatic and nonadiabatic STTs are present, the nonadiabatic STT dominates the domain-wall motion and the intrinsic pinning effect is suppressed, even for a small nonadiabatic coefficient b [6,8].

The sLLG equation on a two-dimensional lattice is numerically integrated with a standard explicit fourth-order Runge-Kutta method with a time step $\Delta t = 0.01$ in units of $(\gamma_0 M_s)^{-1}$. To explore the scaling laws of the creep motion, the dynamic system should be considered in the thermodynamic limit. In our simulations, the antiperiodic and periodic boundary conditions are adopted for the x and y axes, respectively [26,27,44,59–62]. The main results are presented with the lattice size $L_x \times L_y = 256 \times 128$. Additional simulations with the larger lattice sizes $L_x \times L_y = 512 \times 512$ and 256×256 confirm that the finite-size effects are negligible and the lattice size $L_y = 128$ is already large enough to obtain reliable results. Meanwhile, the maximum position of the domain wall in our simulations is always smaller than $L_x = 256$ and it does not reach the boundary. The fluctuations increase as the temperature rises, and the timescale for reaching the steady state increases as the driving force decreases. In order to reduce errors and obtain sufficiently accurate results for the creep exponent and roughness exponent at finite temperatures, the total number of samples of the quenched disorder for the statistical average is over 5000 and the maximum simulation time of one sample is up to 100 000. All the samples are randomly divided into three groups. The roughness exponent and creep exponents are then calculated in each group. The errors, i.e., the standard deviations of the average value, are estimated through the independent measurements in three groups.

In the initial state, a head-to-head domain wall parallel to the y axis lies on the xy plane at the position $x = 16$. The domain wall is smooth without roughness. The initial width of the domain wall is five grids and the results are not sensitive to this initial width. In Fig. 1 the domain-wall structure at $u = 0.10$ and $T = 200$ K is plotted. The arrow represents the local magnetization on the lattice site. For clarity, we draw an arrow every four lattice sites in the y direction. The x component of $\mathbf{m}_i$ is depicted by the grayscale level. In Figs. 1(a) and 1(b) the proportions of the nonadiabatic STT are $b = 0.0$ and 0.1, respectively. When the driving current in the x direction is applied, the domain wall propagates in the x direction; meanwhile, it roughens in the y direction, i.e., the domain-wall profile fluctuates in the y direction, due to the quenched disorder. The domain-wall width may slightly change during the time evolution.

The domain-wall velocity v versus the driving current u for the adiabatic and nonadiabatic STTs at $T = 200$ K is plotted in Fig. 2. In the adiabatic case, there is an intrinsic threshold u_i below which the domain wall does not move at zero temperature even without the disorder. This intrinsic pinning is entirely due to the hard-axis magnetic anisotropy $K_{\perp}$ and does not occur for the field-driven domain-wall motion or the current-driven domain-wall motion with $b \neq 0$. As shown in Fig. 2(a), the intrinsic pinning threshold for a perfect film without the disorder is $u_i = 0.08$. The extrinsic pinning threshold induced by the disorder, i.e., the critical current of the pinning-depinning phase transition at zero temperature, is determined based on the dynamic approach, which has been investigated in previous works [26,28]. Since the fluctuation at zero temperature is much smaller than that at a finite temperature, the total number of samples of the quenched disorder for the statistical average is about 1000. For the domain-wall motion driven by the adiabatic STT, the critical current induced by the disorder is $u_c = 0.48$ for $b = 0.0$. The intrinsic pinning effect is suppressed when the nonadiabatic STT is applied. As shown in Fig. 2(b), the critical current is $u_c = 0.45$ for $b = 0.1$, smaller than the adiabatic one. When $u < u_c$ at a finite temperature, the intrinsic pinning potential induced by the hard-axis anisotropy and the extrinsic pinning potential induced by the disorder are overcome by the thermal effect, resulting in the nonzero velocity of the domain wall. The inset of Fig. 2(a) shows the zoomed-in view of the velocities at low currents.

As shown in Fig. 3, the creep exponents u_a and u_n of the adiabatic and nonadiabatic STTs are accurately measured at different temperatures. In these measurements, Eq. (7) is reformulated as $\ln v \sim u^{-\mu}$, so the creep exponent can be determined from a linear fit in the figure. In the inset, the standard error σ, which quantifies the quality of the linear fit, is plotted as a function of the possible μ. The creep exponents $\mu_a = 0.37(3)$ and $\mu_n = 0.25(2)$ are thus determined from the minimum of σ. Additional simulations for $\alpha = 0.5$ give the same values of the creep exponents within errors, $\mu_a = 0.38(5)$ and $\mu_n = 0.24(3)$, and these results support

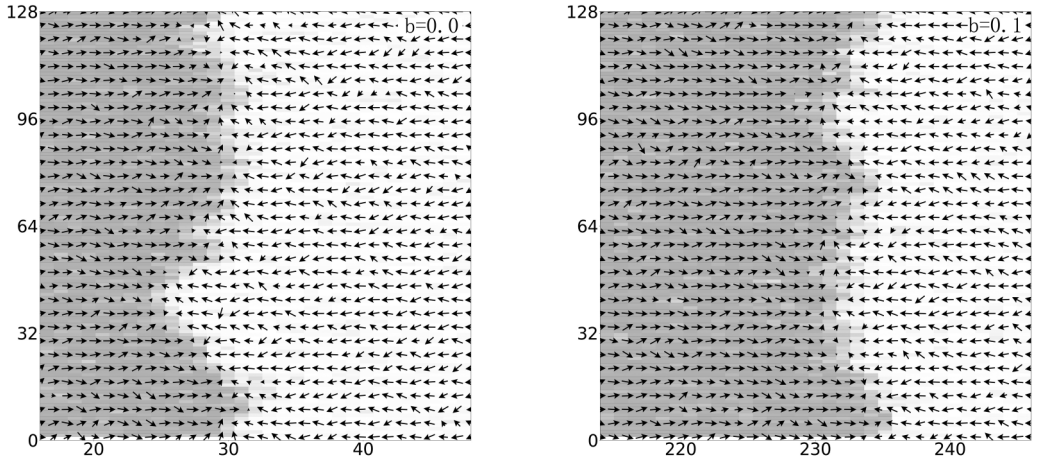

FIG. 1. Domain-wall structures with the driving current $u = 0.10$ at $T = 200$ K and $t = 50\,000$ plotted for the (a) adiabatic ($b = 0.0$) and (b) nonadiabatic ($b = 0.1$) STTs. Arrows represent the projections of $\mathbf{m}_i$ onto the xy plane. The x component of $\mathbf{m}_i$ is depicted by the grayscale level.

that the damping constant does not alter the universality class. Various measurements and calculations of the creep exponent are reported in the experiments and theories. The simplified theory based on elastic domain-wall lines predicts $\mu_a = 0.5$ and $\mu_n = 0.25$ [22]. In most experiments, the adiabatic and nonadiabatic STTs are not clearly distinguished. The nonadiabatic coefficient b in most magnetic materials is not equal to zero, which results in the creep exponent $\mu = 0.23$–0.25 [24,25,37,38,63,64]. Thus, it is reasonable to believe that the nonadiabatic creep exponent μ_n is approximately equal to 0.25. There are at least two independent measurements in the experiments which yield the adiabatic creep exponents $\mu_a = 0.33(6)$ in (Ga,Mn)As [17] and $\mu_a = 0.39(6)$ in Ta/CoFeB/MgO [24]. For comparison, the creep exponent for the field-driven domain-wall motion is $\mu_h = 0.25$ [15–17,19,20].

According to the functional renormalization group theory, the roughness exponent ζ is computed with Eq. (6) from the domain-wall structure in the equilibrium state without the driving force. In order to accurately obtain the roughness exponent, the lattice size $L_x \times L_y = 128 \times 256$ is adopted in the simulation. In Fig. 4(a) the logarithmic roughness function $\ln C(L)$ is plotted against $\ln L$ at different temperatures. When the spatial length $L > 90$, the roughness function $C(L)$ almost reaches the saturation regime and deviates from the power-law behavior [65]. From the slopes of the curves before the saturation regime, one measures $2\zeta = 1.34(4)$. Thus, the equilibrium roughness exponent $\zeta = 0.67(2)$ is obtained.

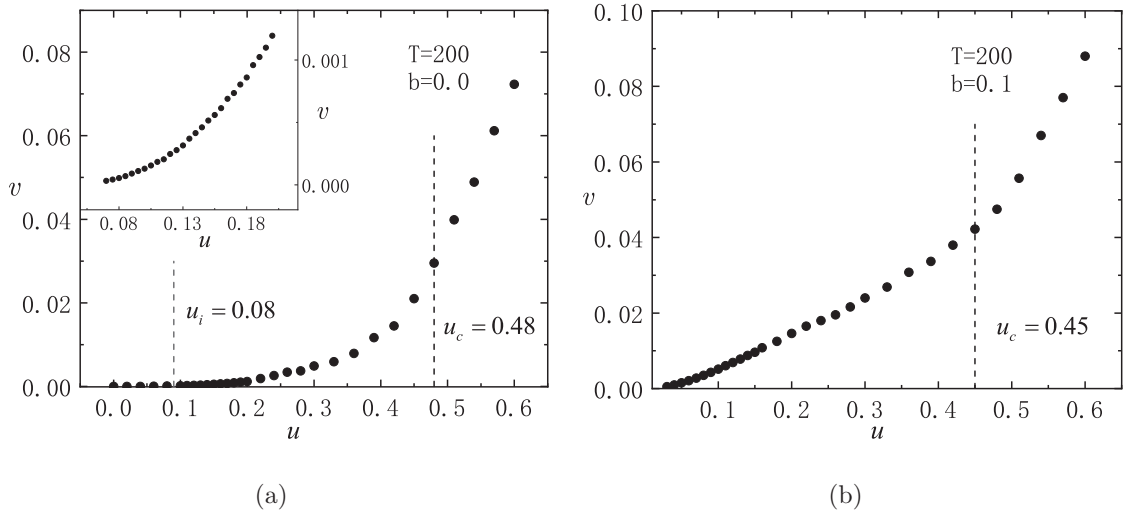

FIG. 2. Domain-wall velocity v versus the driving current u for the (a) adiabatic and (b) nonadiabatic STTs at $T = 200$ K. (a) Adiabatic coefficient $b = 0.0$. The extrinsic pinning threshold induced by the disorder at zero temperature is $u_c = 0.48$. The intrinsic pinning threshold without the disorder is $u_i = 0.08$. In the inset, a close-up plot of the velocity versus the current is shown. (b) Nonadiabatic coefficient $b = 0.1$. The critical current at zero temperature is $u_c = 0.45$. There is no intrinsic pinning.

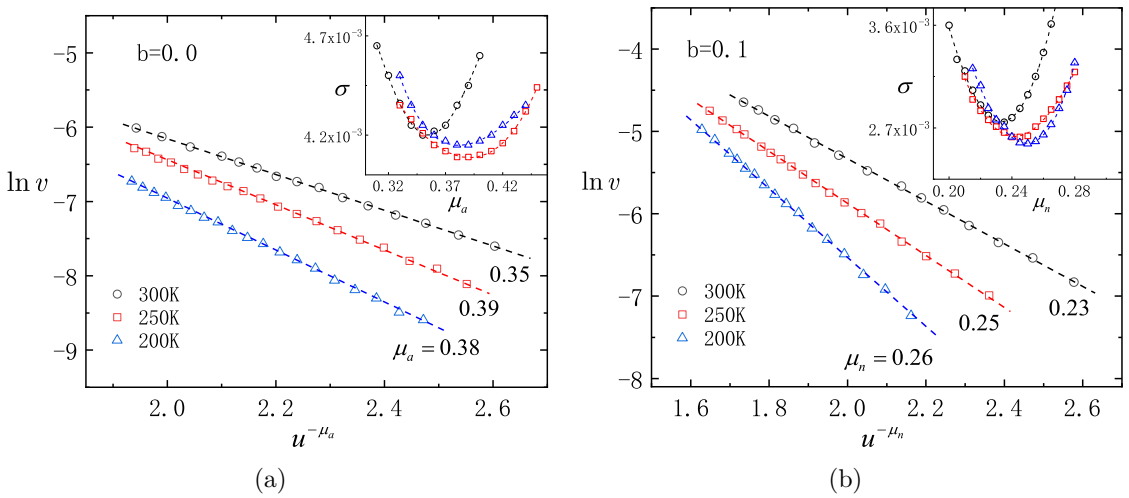

FIG. 3. Logarithmic domain-wall velocity $\ln v$ plotted as a function of $u^{-\mu}$. Error bars are smaller than the symbol sizes. Dashed lines represent the linear fits. The creep exponents (a) μ_a and (b) μ_n are evaluated at different temperatures. The insets of (a) and (b) show the standard error σ of the linear fit.

For comparison, $\zeta = \frac{2}{3}$ was predicted by the theory and $\zeta = 0.5$–0.7 was measured in the experiments [38,42,66–71]. The Curie temperature $T_c = 345$ K is determined with the dynamic approach, which has been verified in our previous work on the order-disorder phase transitions with the sLLG equation [27]. Since the temperature $T = 300$ K is high and closer to $T_c = 345$ K, overhangs and islands are observed in the bulk, which may alter the universality class [72]. This might explain why the creep exponent and the roughness exponent at $T = 300$ K slightly deviate from those at $T = 250$ and 200 K. The roughness exponent as a function of the driving current u for the adiabatic and nonadiabatic STTs is plotted in Fig. 4(b). Generally speaking, the roughness exponent decreases as the driving force increases. The values for $b = 0.0$ are larger than those for $b = 0.1$ at the same driving current u in the entire creep region. The roughness exponent seems to be constant for $b = 0.0$ in the region $u < 0.06$, where the driving force could not overcome the intrinsic pinning potential, resulting in no rotations and movements of the domain wall. This behavior is almost as if there were no driving force. For $b = 0.0$ with $u > 0.06$, the rotation of the domain wall and the variation of the tilting angle are observed. Compared with the nonadiabatic case at $b = 0.1$, the roughness exponent at $b = 0.0$ decreases more slowly as u increases.

With the equilibrium roughness exponent $\zeta = 0.67(2)$ as input, the scaling relations in Eqs. (8) and (9) yield $\mu_a = 0.52(2)$ and $\mu_n = 0.26(1)$. Compared with our numerical results $\mu_a = 0.37(3)$ and $\mu_n = 0.25(2)$, the scaling relation holds for the nonadiabatic exponents, but it is invalid for the adiabatic ones. In order to explain this unexpected result, we focus on the tilting angle θ of the domain wall. In the initial state, the domain wall lies on the xy plane, i.e., the tilting angle of the domain wall is zero. As time evolves, however, the tilting angle θ changes; this is shown in Fig. 5. For the

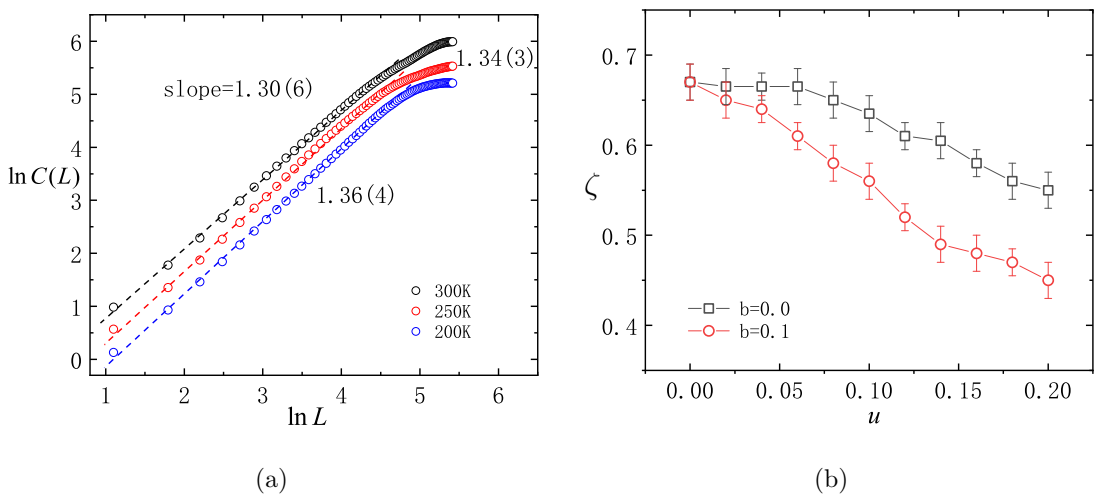

FIG. 4. (a) Logarithmic roughness function $\ln C(L)$ plotted against $\ln L$ at different temperatures. Dashed lines are the linear fits. Error bars are smaller than the symbol sizes. (b) Roughness exponent plotted as a function of the driving current for the adiabatic and nonadiabatic STTs. Each error bar corresponds to the standard deviation of the average value.

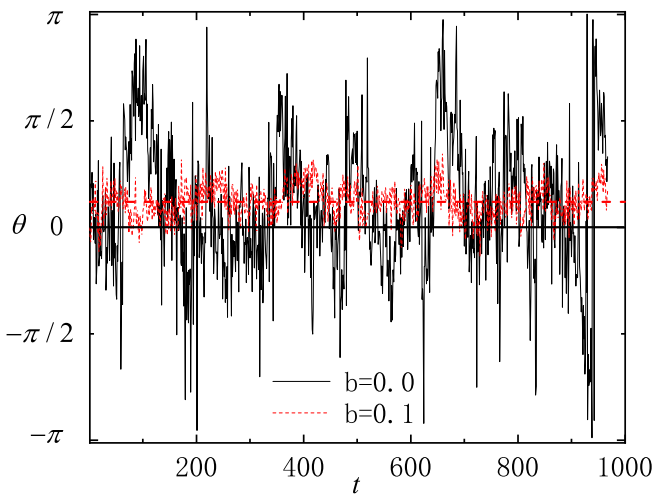

FIG. 5. Tilting angle θ of the domain wall versus the time t at $T = 200$ K and $u = 0.1$ for the adiabatic and the nonadiabatic STTs. For $b = 0.0$, as shown by the black solid line, the domain wall keeps rotating along the x axis. For $b = 0.1$, the tilting angle θ represented by the red dashed line only fluctuates near the equilibrium angle $\langle\theta\rangle = 0.37$. The red dashed horizontal lines shows the value 0.37.

adiabatic case ($b = 0.0$), θ varies between $-\pi$ and π. Therefore, the domain wall keeps rotating along the x axis all the time. There exists an extra degree of freedom, i.e., the tilting angle θ of the domain wall, for the domain-wall motion driven by the adiabatic STT. In other words, to overcome the intrinsic pinning barrier, the domain wall will rotate while moving, whereas for the nonadiabatic case ($b = 0.1$), the tilting angle is bound at a fixed value $\langle\theta\rangle = 0.37$, which is similar to that of the domain wall driven by the magnetic field. The thermal effect just makes the angle fluctuate around the steady value of the angle. This indicates that the rotation of the domain wall is the main mechanism leading to the violation of the scaling relation for μ_a in Eq. (8).

There have been some theoretical analyses on the domain-wall creep motion based on the sLLG equation [22,23]. For simplification, however, the domain-wall motion is analyzed under certain assumptions or approximations, such as the amplitude of the tilting angle being much smaller than π or the disorder coupling only to the domain-wall position, not to its tilting angle. These assumptions or approximations may be valid to some extent only for the creep motion of the domain wall driven by the magnetic field or the nonadiabatic STT. The new degree of freedom, i.e., the tilting angle of the domain wall, has not been fully considered. In fact, the tilting angle of the domain wall is significantly affected by the disorder in the creep motion driven by the adiabatic STT. On the other hand, the domain wall was simplified to a single-value elastic line or a rigid body without a width variation in Refs. [22,23]. Hence, the dynamic effects of overhangs and islands are ignored, which may also modify the universality class. All these reasons explain why our numerical simulations yield a different creep exponent $\mu_a = 0.37(3)$.

Theoretically, the universality class and the creep exponent are generally believed to be determined only by the symmetry, the spatial dimension, the correlation of the disorder, the driving force, etc. [22,23,58]. For example, it has been demonstrated that the types of domain wall do not alter the universality class [23], although the magnetostatic interaction determines whether the steady state is a Néel domain wall or a Bloch domain wall. The parameters of the materials and some specific realizations in our simulations, such as the type of domain wall and the direction that the material is magnetized, are different from those of previous experiments; it is still meaningful to compare our results with the experimental and theoretical ones, at least in the sense of the universality classes. In fact, as discussed above, the theoretical models in Refs. [22,23] are also simplified. Nevertheless, all the theoretical, the experimental, and our numerical results give the consistent values for the nonadiabatic creep exponent μ_n, in the same universality class of the field-driven domain-wall motion. However, the adiabatic creep exponent μ_a obtained in our numerical simulation is close to the experimental results, rather than that predicted by the theoretical analysis [22].

IV. SUMMARY

We have performed numerical simulations of the SLLG equation to investigate the creep motion of the domain wall driven by the adiabatic and the nonadiabatic STTs in a disordered film. From the scaling behaviors of the creep motion, the adiabatic and nonadiabatic creep exponents as well as the roughness exponents are accurately determined. The nonadiabatic creep exponent $\mu_n = 0.25(2)$ is consistent within errors with the creep exponent $\mu_h = 0.25$ for the magnetic field. However, the adiabatic creep exponent $\mu_a = 0.37(3)$ belongs to a different universality class. These results from our simulations are comparable to the experimental measurements $\mu_a = 0.33$–0.39 and $\mu_n = 0.23$–0.25, but go beyond the existing theoretical analysis under certain assumptions or approximations. Further, the domain-wall tilting angles for the adiabatic and nonadiabatic STTs are respectively measured, which indicates that the disorder-induced pinning effect on the domain-wall rotation cannot be ignored in the theoretical analysis and it leads to the difference between the adiabatic and the nonadiabatic creep exponents.

ACKNOWLEDGMENTS

This work was supported in part by National Natural Science Foundation of China under Grants No. 11775186, No. 11874135, and No. 11875120, Zhejiang Provincial Natural Science Foundation under Grants No. LY17A050002 and No. LQ21A050001, and Key Research and Development Program of Zhejiang Province under Grant No. 2021C01039.

[1] S. Krause, G. Herzog, T. Stapelfeldt, L. B. Berbil-Bautista, M. Bode, E. Y. Vedmedenko, and R. Wiesendanger, Phys. Rev. Lett. **103**, 127202 (2009).

[2] D. A. Allwood, G. Xiong, C. C. Faulkner, D. Atkinson, D. Petit, and R. P. Cowburn, Science **309**, 1688 (2005).

[3] S. Parkin and S. H. Yang, Nat. Nanotechnol. **10**, 195 (2015).

[4] J. Grollier, D. Querlioz, K. Y. Camsari, K. Everschor-Sitte, S. Fukami, and M. D. Stiles, Nat. Electron. **3**, 360 (2020).

[5] J. Torrejon, M. Riou, F. A. Araujo, S. Tsunegi, G. Khalsa, D. Querlioz, P. Bortolotti, V. Cros, K. Yakushiji, A. Fukushima, H. Kubota, S. Yuasa, M. D. Stiles, and J. Grollier, Nature (London) **547**, 428 (2017).

[6] S. Zhang and Z. Li, Phys. Rev. Lett. **93**, 127204 (2004).

[7] J. He, Z. Li, and S. Zhang, J. Appl. Phys. **98**, 016108 (2005).

[8] A. Thiaville, Y. Nakatani, J. Miltat, and Y. Suzuki, Europhys. Lett. **69**, 990 (2005).

[9] T. Koyama, D. Chiba, K. Ueda, K. Kondou, H. Tanigawa, S. Fukami, T. Suzuki, N. Ohshima, N. Ishiwata, Y. Nakatani, K. Kobayashi, and T. Ono, Nat. Mater. **10**, 194 (2011).

[10] G. Tatara and H. Kohno, Phys. Rev. Lett. **92**, 086601 (2004).

[11] L. Fan, J. Hu, Y. Su, and J. Zhu, J. Magn. Magn. Mater. **401**, 484 (2016).

[12] S. Parkin, M. Hayashi, and L. Thomas, Science **320**, 190 (2008).

[13] I. M. Miron, T. Moore, H. Szambolics, L. D. Buda-Prejbeanu, S. Auffret, B. Rodmacq, S. Pizzini, J. Vogel, M. Bonfim, A. Schuhl, and G. Gaudin, Nat. Mater. **10**, 419 (2011).

[14] S. Vélez, J. Schaab, M. S. Wörnle, M. Müller, E. Gradauskaite, P. Welter, C. Gutgsell, C. Nistor, C. L. Degen, M. Trassin, M. Fiebig, and P. Gambardella, Nat. Commun. **10**, 4750 (2019).

[15] S. Lemerle, J. Ferré, C. Chappert, V. Mathet, T. Giamarchi, and P. Le Doussal, Phys. Rev. Lett. **80**, 849 (1998).

[16] F. Cayssol, D. Ravelosona, C. Chappert, J. Ferré, and J. P. Jamet, Phys. Rev. Lett. **92**, 107202 (2004).

[17] M. Yamanouchi, J. Ieda, F. Matsukura, S. E. Barnes, S. Maekawa, and H. Ohno, Science **317**, 1726 (2007).

[18] A. Kanda, A. Suzuki, F. Matsukura, and H. Ohno, Appl. Phys. Lett. **97**, 032504 (2010).

[19] J.-C. Lee, K.-J. Kim, J. Ryu, K.-W. Moon, S.-J. Yun, G.-H. Gim, K.-S. Lee, K.-H. Shin, H.-W. Lee, and S.-B. Choe, Phys. Rev. Lett. **107**, 067201 (2011).

[20] J. Gorchon, S. Bustingorry, J. Ferré, V. Jeudy, A. B. Kolton, and T. Giamarchi, Phys. Rev. Lett. **113**, 027205 (2014).

[21] T. Tybell, P. Paruch, T. Giamarchi, and J.-M. Triscone, Phys. Rev. Lett. **89**, 097601 (2002).

[22] R. A. Duine and C. M. Smith, Phys. Rev. B **77**, 094434 (2008).

[23] J. Ryu, S.-B. Choe, and H.-W. Lee, Phys. Rev. B **84**, 075469 (2011).

[24] S. DuttaGupta, S. Fukami, C. Zhang, H. Sato, M. Yamanouchi, F. Matsukura, and H. Ohno, Nat. Phys. **12**, 333 (2016).

[25] S. DuttaGupta, S. Fukami, B. Kuerbanjiang, H. Sato, F. Matsukura, V. K. Lazarov, and H. Ohno, AIP Adv. **7**, 055918 (2017).

[26] L. Xiong, B. Zheng, M. H. Jin, L. Wang, and N. J. Zhou, New J. Phys. **20**, 023027 (2018).

[27] M. H. Jin, B. Zheng, L. Xiong, N. J. Zhou, and L. Wang, Phys. Rev. E **98**, 022126 (2018).

[28] M. H. Jin, N. J. Zhou, L. Xiong, and B. Zheng, J. Stat. Mech. (2019) 053303.

[29] L. Xiong, B. Zheng, M. H. Jin, and N. J. Zhou, Phys. Rev. B **100**, 064426 (2019).

[30] L. Xiong, B. Zheng, M. H. Jin, and N. J. Zhou, New J. Phys. **22**, 033043 (2020).

[31] Y. Saito, Y. M. Itahashi, T. Nojima, and Y. Iwasa, Phys. Rev. Mater. **4**, 074003 (2020).

[32] C. Reichhardt, D. Ray, and C. J. O. Reichhardt, Phys. Rev. Lett. **114**, 217202 (2015).

[33] C. Reichhardt and C. J. O. Reichhardt, J. Phys.: Condens. Matter **31**, 07LT01 (2018).

[34] E. E. Ferrero, L. Foini, T. Giamarchi, A. B. Kolton, and A. Rosso, Phys. Rev. Lett. **118**, 147208 (2017).

[35] R. Willa, J. A. Galvis, J. Benito-Llorens, E. Herrera, I. Guillamon, and H. Suderow, Phys. Rev. Res. **2**, 013125 (2020).

[36] Y. Y. He, B. Zheng, and N. J. Zhou, Phys. Rev. B **94**, 134302 (2016).

[37] L. San Emeterio Alvarez, K.-Y. Wang, S. Lepadatu, S. Landi, S. J. Bending, and C. H. Marrows, Phys. Rev. Lett. **104**, 137205 (2010).

[38] R. Díaz Pardo, N. Moisan, L. J. Albornoz, A. Lemaître, J. Curiale, and V. Jeudy, Phys. Rev. B **100**, 184420 (2019).

[39] A. J. Schellekens, A. van den Brink, J. H. Franken, H. J. M. Swagten, and B. Koopmans, Nat. Commun. **3**, 847 (2012).

[40] E. Martinez, J. Phys.: Condens. Matter **24**, 024206 (2011).

[41] B. Cui, H. Wu, M. Chang, J. Yun, Y. Zuo, M. Gao, K. L. Wang, and L. Xi, J. Magn. Magn. Mater. **493**, 165676 (2020).

[42] D. Jordán, L. J. Albornoz, J. Gorchon, C. H. Lambert, S. Salahuddin, J. Bokor, J. Curiale, and S. Bustingorry, Phys. Rev. B **101**, 184431 (2020).

[43] P. J. Metaxas, J. P. Jamet, A. Mougin, M. Cormier, J. Ferré, V. Baltz, B. Rodmacq, B. Dieny, and R. L. Stamps, Phys. Rev. Lett. **99**, 217208 (2007).

[44] L. D. Geng and Y. M. Jin, Europhys. Lett. **116**, 36002 (2016).

[45] D. Wei, J. Song, and C. Liu, IEEE Trans. Magn. **52**, 7100808 (2016).

[46] D. Hinzke and U. Nowak, Phys. Rev. Lett. **107**, 027205 (2011).

[47] Y. Yuksel, E. Vatansever, and H. Polat, J. Phys.: Condens. Matter **24**, 436004 (2012).

[48] F. Schlickeiser, U. Ritzmann, D. Hinzke, and U. Nowak, Phys. Rev. Lett. **113**, 097201 (2014).

[49] M. O. A. Ellis and R. W. Chantrell, Appl. Phys. Lett. **106**, 162407 (2015).

[50] S. A. Bender, H. Skarsvåg, A. Brataas, and R. A. Duine, Phys. Rev. Lett. **119**, 056804 (2017).

[51] R. Bastardis, U. Atxitia, O. Chubykalo-Fesenko, and H. Kachkachi, Phys. Rev. B **86**, 094415 (2012).

[52] X. S. Wang and X. R. Wang, Phys. Rev. B **90**, 014414 (2014).

[53] Y. H. Shen, X. S. Wang, and X. R. Wang, Phys. Rev. B **94**, 014403 (2016).

[54] C. Reichhardt and C. J. O. Reichhardt, Rep. Prog. Phys. **80**, 026501 (2016).

[55] W. F. Brown, Phys. Rev. **130**, 1677 (1963).

[56] R. F. L. Evans, W. J. Fan, P. Chureemart, T. A. Ostler, M. O. A. Ellis, and R. W. Chantrell, J. Phys.: Condens. Matter **26**, 103202 (2014).

[57] Y.-P. Zhao, G. Palasantzas, G.-C. Wang, and J. T. M. De Hosson, Phys. Rev. B **60**, 1216 (1999).

[58] P. Chauve, T. Giamarchi, and P. Le Doussal, Phys. Rev. B **62**, 6241 (2000).

[59] X. P. Qin, B. Zheng, and N. J. Zhou, J. Phys. A: Math. Theor. **45**, 115001 (2012).

[60] B. Xi, M.-B. Luo, V. M. Vinokur, and X. Hu, Sci. Rep. **5**, 14062 (2015).

[61] V. Boddu, F. Endres, and P. Steinmann, Sci. Rep. **7**, 806 (2017).

[62] K. Hukushima, Phys. Rev. E **60**, 3606 (1999).

[63] V. Jeudy, R. Díaz Pardo, W. Savero Torres, S. Bustingorry, and A. B. Kolton, Phys. Rev. B **98**, 054406 (2018).
[64] C. Burrowes, D. Ravelosona, C. Chappert, S. Mangin, E. E. Fullerton, J. A. Katine, and B. D. Terris, Appl. Phys. Lett. **93**, 172513 (2008).
[65] P. Paruch, A. B. Kolton, X. Hong, C. H. Ahn, and T. Giamarchi, Phys. Rev. B **85**, 214115 (2012).
[66] W. S. Torres, R. D. Pardo, S. Bustingorry, A. B. Kolton, A. Lemaître, and V. Jeudy, Phys. Rev. B **99**, 201201(R) (2019).
[67] J. Guyonnet, E. Agoritsas, S. Bustingorry, T. Giamarchi, and P. Paruch, Phys. Rev. Lett. **109**, 147601 (2012).
[68] B. Ziegler, K. Martens, T. Giamarchi, and P. Paruch, Phys. Rev. Lett. **111**, 247604 (2013).
[69] N. A. Pertsev, D. A. Kiselev, I. K. Bdikin, M. Kosec, and A. L. Kholkin, J. Appl. Phys. **110**, 052001 (2011).
[70] K.-W. Moon, D.-H. Kim, S.-C. Yoo, C.-G. Cho, S. Hwang, B. Kahng, B.-C. Min, K.-H. Shin, and S.-B. Choe, Phys. Rev. Lett. **110**, 107203 (2013).
[71] G. Catalan, H. Béa, S. Fusil, M. Bibes, P. Paruch, A. Barthélémy, and J. F. Scott, Phys. Rev. Lett. **100**, 027602 (2008).
[72] N. J. Zhou and B. Zheng, Phys. Rev. E **82**, 031139 (2010).